Mechanics of Advanced Materials and Structures

ISSN: 1537-6494 (Print) 1537-6532 (Online) Journal homepage: https://www.tandfonline.com/loi/umcm20

Tunable flexural wave band gaps in a prestressed elastic beam with periodic smart resonators

Weijian Zhou, Bin Wu, Yipin Su, Dongying Liu, Weiqiu Chen & Ronghao Bao

MECHANICS OF ADVANCED MATERIALS AND STRUCTURES
https://doi.org/10.1080/15376494.2018.1553261

ORIGINAL ARTICLE

Tunable flexural wave band gaps in a prestressed elastic beam with periodic smart resonators

Weijian Zhou[a], Bin Wu[a], Yipin Su[a], Dongying Liu[b], Weiqiu Chen[a,c,d], and Ronghao Bao[a,c,d]

[a]Department of Engineering Mechanics, Zhejiang University Hangzhou, China; [b]School of Civil Engineering, Guangzhou University, Guangzhou, China; [c]State Key Lab of CAD & CG, Zhejiang University, Zijingang Campus, Hangzhou, China; [d]Key Laboratory of Soft Machines and Smart Devices of Zhejiang Province, Zhejiang University, Hangzhou, China

ABSTRACT
This paper theoretically studies the propagation of flexural waves in an actively controllable locally resonant (LR) beam. It is shown that the band gaps can be simultaneously tuned by the axial force and the active electrical control actions. In some special cases, a super-wide pseudo-gap resulted from the combination of the resonance and Bragg gaps can be observed. The condition of inducing such pseudo-gap is further obtained with a closed-form expression with respect to the electrical control parameter and the axial force, which can be explored to actively control the broadband pseudo-gap by tuning these two parameters.

ARTICLE HISTORY
Received 25 November 2018
Accepted 25 November 2018

KEYWORDS
Local resonance; band gap; active control; prestress; pseudo-gap

1. Introduction

In the last few years, a variety of attentions have been focused on the control, direction and manipulation of elastic/acoustic waves in phononic crystals (PCs), the artificially designed composites mainly consisting of a periodic array of elastic scatters embedded in a host matrix with high impedance contrast between scatters and matrix [1–13]. Owing to their novel and unique properties (band gaps and negative refraction etc.) usually not available in nature, PCs have the promising applications as frequency filters, acoustic barriers, vibration isolators, wave guiding, novel transducers, and so on.

One of the most important properties of PCs is the existence of band gaps, within which the elastic waves are prohibited to propagate through the structures by Bragg scattering or/and local resonance (LR). The Bragg band gap is a result of destructive interference between the scattered waves with the periodic scatters embedded in matrix, while the LR band gap is caused by the coupling between the propagating waves along the matrix and the localized mode of the scatters. With different mechanism, the lowest frequency of the LR band could be two orders of magnitude lower than that of the Bragg band [6], making it more feasible to engineer PCs with low frequency through LR than Bragg scattering. Furthermore, recent investigations have shown that deliberately tailored LR PCs could possess more novel properties, such as negative modulus [14] and [15], negative mass density [16], and double negative parameters [8].

Tunability of band gaps in PCs to comply with varying requirements needs becomes a new topic in recent years, and a lot of valuable researches have been reported through external stimuli, such as mechanical loading [17–19], electric field [20–22], and magnetic field [23]. Gei et al. [24] found that the tensile (compressive) prestress applied on the PCs could increase (decrease) the frequency ranges of band gaps, indicating that the prestress is a feasible way to control the location of band gaps. Galich et al. [25] analytically studied the wave propagation in layered hyperelastic composites and concluded that band gaps could be largely tuned by the large deformation. Furthermore, large deformation together with material heterogeneity may induce elastic instabilities, leading to dramatic microstructure transformations [26]. Recently, this strategy has been employed to achieve remarkably tunable soft PCs [27–29]. On the other hand, by combining the smart materials with the active control technology, band gaps in PCs can be actively controlled [30].

In a LR plate, a super-wide pseudo-gap, which is formed by a combination of LR gap and Bragg gap, may emerge when the pass band between the two gaps is extremely narrow [31]. This phenomenon was also observed in one-dimensional LR PCs [32]. Controllable broadband pseudo-gaps are highly desired by engineers and may have many potential applications in the designs of tunable energy harvesters, active frequency filters, smart transducers, and so on. In this paper, we will present an effective method to control the pseudo-gap in a prestressed beam attached with periodic smart resonators (electrically controlled piezoelectric spring-mass oscillators). The influences of the axial force and the active electrical control actions (AECAs) on the Bragg gap and LR gap will be discussed in detail. We find that the Bragg gap relies on the axial force while the LR gap is significantly influenced by the AECAs on the resonators.

CONTACT Ronghao Bao brh@zju.edu.cn Department of Engineering Mechanics, Zhejiang University, Hangzhou 310027, China.
Color versions of one or more of the figures in the article can be found online at www.tandfonline.com/umcm.

Thus, an actively tunable super-wide pseudo-gap may be achieved when the axial force and/or the AECAs are deliberately controlled.

The paper is organized as follows. First, the explicit dispersion relation of the prestressed smart LR beam is derived by the transfer matrix method (TMM). The gap edge frequencies (GEFs) are solved explicitly from the dispersion equation. Then, the condition of inducing pseudo-gap is obtained with a closed-form expression with respect to the axial force and the AECAs. Numerical simulations are finally conducted to show that both the axial force and the AECAs have significant effects on the properties of band gaps. In particular, an actively tunable super-wide pseudo-gap is observed, and its width and position increase with the axial force. It is expected that this result can be applied to engineer tunable acoustic metamaterials possessing super-wide band gaps in the low frequency range.

2. Dispersion characteristics of a prestressed smart LR beam

2.1. The beam structure

The smart LR beam considered in this work is a homogeneous thin Euler-Bernoulli beam periodically attached with smart resonators, as sketched in Figure 1a. Each resonator consists of a lumped mass connected to the beam with a piezoelectric spring whose stiffness can be actively controlled [30]. The lattice constant (spacing between two adjacent resonators) of the periodic structure is L, and the width and thickness of the beam are H and b, respectively. m_R and k_R are the lumped mass and the electrically controllable stiffness of the piezoelectric spring, respectively. The beam is subjected to an axial force N. AECAs are usually applied on the piezoelectric springs to tune their stiffness as well. A unit cell of the structure is schematically shown in Figure 1b.

2.2. Characterization of the resonator

The constitutive equations of the piezoelectric spring are given by [30]

$$\begin{Bmatrix} E_p \\ \sigma_p \end{Bmatrix} = \begin{bmatrix} 1/\kappa_p & -h_p \\ -h_p & C^D \end{bmatrix} \begin{Bmatrix} D_p \\ S_p \end{Bmatrix} \tag{1}$$

where E_p, D_p, σ_p and S_p are the electrical field intensity, electrical displacement, stress, and strain of the piezoelectric spring, whilst κ_p, h_p, and C^D are the electrical permittivity, piezoelectric stiffness, and elastic modulus of the piezoelectric spring, respectively.

Assuming that the width, thickness and length of the piezoelectric spring are b_p, t_p, and l_p, respectively, we can express Eq. (1) as

$$\begin{Bmatrix} V/t_p \\ F_p/b_p t_p \end{Bmatrix} = \begin{bmatrix} 1/\kappa_p & -h_p \\ -h_p & C^D \end{bmatrix} \begin{Bmatrix} Q_p/b_p l_p \\ (z_{uj} - z_{dj})/l_p \end{Bmatrix} \tag{2}$$

where V, F_p, and Q_p are the applied voltage, piezo-force, and charge respectively. z_{uj} and z_{dj} represent the displacement of the lump mass and deflection of the beam at the connection point of the jth cell repectively. Therefore $z_{uj} - z_{dj}$ is the net displacement of the piezoelectric spring. By eliminating the charge Q_p in Eq. (2), we obtain

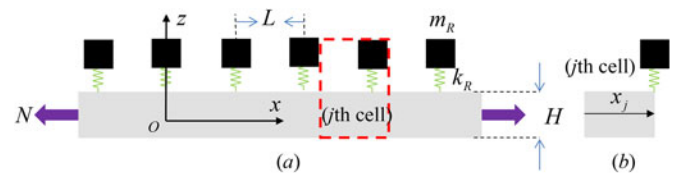

Figure 1. Schematics of a thin beam with oscillators.

$$F_p = -h_p \varepsilon^S b V_p + \left[\frac{b t_p \left(C^D - h_p^2 \varepsilon^S \right)}{l_p} \right] (z_{uj} - z_{dj}) \tag{3}$$

Let the voltage V_p be generated by the following feedback control law

$$V_p = -K_g (z_{uj} - z_{dj}) \tag{4}$$

where K_g is the control gain to be determined by the requirement. Then, the piezo-force can be expressed by

$$F_p = k_R (z_{uj} - z_{dj}) \tag{5}$$

where the total stiffness of the piezoelectric spring k_R is

$$k_R = k_{ss} + k_{as} \tag{6}$$

with $k_{as} \equiv h_p \varepsilon^S b K_g$ being the active stiffness due to control gain and $k_{ss} \equiv b t_p (C^D - h_p^2 \varepsilon^S)/l_p$ being the original passive structural stiffness of the piezoelectric spring, respectively.

2.3. Transfer matrix method

For a time-harmonic flexural wave in the form of $e^{-i\omega t} w(x)$ traveling along the beam with initial axial force N, the deflection of the beam $w(x)$ should satisfy the following differential equation [24]

$$EI \frac{d^4 w}{dx^4} - N \frac{d^2 w}{dx^2} - \rho A \omega^2 w = 0 \tag{7}$$

where ω is the angular frequency, ρ and E are the mass density and Young's modulus of the beam, A is the cross-sectional area and I is the area moment of inertia with respect to the neutral axis of bending, respectively, and $i = \sqrt{-1}$. The solution of $w(x)$ reads as

$$w(x) = W_1 \cos \lambda x + W_2 \sin \lambda x + W_3 \cosh \gamma x + W_4 \sinh \gamma x \tag{8}$$

where

$$\lambda = \sqrt{\frac{-N + \sqrt{N^2 + 4EI\rho A \omega^2}}{2EI}}, \gamma = \sqrt{\frac{N + \sqrt{N^2 + 4EI\rho A \omega^2}}{2EI}} \tag{9}$$

and the coefficients, $W_i (i = 1, 2, 3, 4)$, are to be determined with the proper boundary conditions (periodicity condition for an infinite beam).

For the jth LR cell, by introducing the local coordinate $x_j = x - jL$, the state vector of the jth LR cell, i.e. $\mathbf{V}_j(x_j) = [\,w_j(x_j) \quad w'_j(x_j) \quad w''_j(x_j) \quad w'''_j(x_j)\,]^T$, can be written as

$$\mathbf{V}_j(x_j) = \mathbf{T}(x_j)\mathbf{W}_j \tag{10}$$

where $w_j(x_j)$ is the beam deflection of the jth LR cell, the superscript 'T' denotes the transpose of a matrix (vector), the prime indicates the derivative with respect to the local coordinate x_j, and

$$\mathbf{T}(x_j) = \begin{bmatrix} \cos\lambda x_j & \sin\lambda x_j & \cosh\gamma x_j & \sinh\gamma x_j \\ -\lambda\sin\lambda x_j & \lambda\cos\lambda x_j & \gamma\sinh\gamma x_j & \gamma\cosh\gamma x_j \\ -\lambda^2\cos\lambda x_j & -\lambda^2\sin\lambda x_j & \gamma^2\cosh\gamma x_j & \gamma^2\sinh\gamma x_j \\ \lambda^3\sin\lambda x_j & -\lambda^3\cos\lambda x_j & \gamma^3\sinh\gamma x_j & \gamma^3\cosh\gamma x_j \end{bmatrix} \tag{11}$$

$$\mathbf{W}_j = \left[\, W_1^{(j)} \quad W_2^{(j)} \quad W_3^{(j)} \quad W_4^{(j)} \,\right]^T \tag{12}$$

The state vector at $x_j = 0$ can be written as

$$\mathbf{V}_j(0) = \mathbf{T}(0)\mathbf{W}_j \tag{13}$$

and the state vector at $x_j = L$ is

$$\mathbf{V}_j(L) = \mathbf{T}(L)\mathbf{W}_j \tag{14}$$

Provided F_p and z_{uj} in Eq. (5) are time-harmonic with the same angular frequency ω, i.e.,

$$F_p = f_j e^{-\mathrm{i}\omega t},\; z_{uj} = v_j e^{-\mathrm{i}\omega t} \tag{15}$$

the equilibrium equation of the lump mass can be expressed as

$$f_j + m_R\omega^2 v_j = 0 \tag{16}$$

and Eq. (5) can be written as

$$f_j = k_R\left(v_j - w_j(L)\right) \tag{17}$$

By eliminating v_j in Eqs. (16) and (17), f_j can be obtained as

$$f_j = -k_R\frac{m_R\omega^2}{k_R - m_R\omega^2}w_j(L) \tag{18}$$

In the case of perfect bonding between the jth cell and the $(j+1)$th cell, the following continuity conditions of displacement, slope, bending moment, and shear force must be satisfied

$$\begin{aligned} w_{j+1}(0) &= w_j(L) \\ w'_{j+1}(0) &= w'_j(L) \\ -EIw''_{j+1}(0) &= -EIw''_j(L) \\ -EIw'''_{j+1}(0) &= -EIw'''_j(L) - \frac{k_R m_R\omega^2}{k_R - m_R\omega^2}w_j(L) \end{aligned} \tag{19}$$

Equation (19) can be rewritten in the form of state vectors

$$\mathbf{V}_{j+1}(0) = \mathbf{P}\mathbf{V}_j(L) \tag{20}$$

where

$$\mathbf{P} = \begin{bmatrix} 1 & 0 & 0 & 0 \\ 0 & 1 & 0 & 0 \\ 0 & 0 & 1 & 0 \\ -D_R & 0 & 0 & 1 \end{bmatrix} \tag{21}$$

and

$$D_R = \frac{k_R m_R\omega^2}{EI(m_R\omega^2 - k_R)} \tag{22}$$

Combining Eqs. (13), (14), and (20) leads to

$$\mathbf{V}_{j+1}(0) = \mathbf{P}\mathbf{T}(L)\mathbf{T}^{-1}(0)\mathbf{V}_j(0) \tag{23}$$

Consequently, for the elastic wave propagation along an infinite periodic beam, the state vectors at the boundaries of the unit cell should be related through the Bloch theorem [33], i.e.,

$$\mathbf{V}_{j+1}(0) = e^{ikL}\mathbf{V}_j(0) \tag{24}$$

where the Bloch wave number k is to be determined when the angular frequency ω is given.

By inserting Eq. (23) into Eq. (24), nontrivial solutions can be acquired when

$$|\mathbf{P}\mathbf{T}(L)\mathbf{T}^{-1}(0) - e^{ikL}\mathbf{I}| = 0 \tag{25}$$

where $\mathbf{I}$ is the 4×4 identity matrix. The explicit expression of Eq. (25) is

$$\cosh^2(ikL) + \alpha_1\cosh(ikL) + \alpha_2 = 0 \tag{26}$$

where

$$\begin{aligned} \alpha_1 &= -[\cos(\lambda L) + \cosh(\gamma L)] - \frac{D_R\gamma\sin(\lambda L) - D_R\lambda\sinh(\gamma L)}{2(\gamma^2+\lambda^2)\lambda\gamma} \\ \alpha_2 &= \cos(\lambda L)\cosh(\gamma L) + \frac{D_R\gamma\sin(\lambda L)\cosh(\gamma L) - D_R\lambda\cos(\lambda L)\sinh(\gamma L)}{2(\gamma^2+\lambda^2)\lambda\gamma} \end{aligned} \tag{27}$$

Specially, when the axial force is removed, i.e. $N = 0$, the dispersion Eq. (26) is consistent with Eq. (36) in Ref. [31].

Obviously, Eq. (26) has the following two solutions:

$$\begin{aligned} k_1 &= -\frac{\mathrm{i}}{L}\cos h^{-1}\left(\frac{-\alpha_1 - \sqrt{\alpha_1^2 - 4\alpha_2}}{2}\right) \\ k_2 &= -\frac{\mathrm{i}}{L}\cos h^{-1}\left(\frac{-\alpha_1 + \sqrt{\alpha_1^2 - 4\alpha_2}}{2}\right) \end{aligned} \tag{28}$$

According to Refs. [32] and [34], the gap edge frequencies (GEFs) of the prestressed LR beam can be obtained from

$$\cos(kL) = \pm 1 \tag{29}$$

By inserting Eq. (29) into Eq. (26), two groups of GEFs can be found. The first group is determined by

$$\cos(\lambda L) = \pm 1 \tag{30}$$

which gives the Bragg frequencies as

$$\omega_{B,n} = \sqrt{\frac{\left[2EI(n\pi/L)^2 + N\right]^2 - N^2}{4\rho AEI}}\;(n = 1, 2, 3, \ldots). \tag{31}$$

The second group is represented by the following two equations:

$$\omega_R^{-2} - \omega^{-2} = \frac{m_R[\lambda \tanh(\gamma L/2) - \gamma \tan(\lambda L/2)]}{2EI\lambda\gamma(\gamma^2 + \lambda^2)} \tag{32}$$

and

$$\omega_R^{-2} - \omega^{-2} = \frac{m_R[\lambda \coth(\gamma L/2) + \gamma \cot(\lambda L/2)]}{2EI\lambda\gamma(\gamma^2 + \lambda^2)} \tag{33}$$

where $\omega_R = \sqrt{k_R/m_R}$. When the axial force is removed, one has $\gamma = \lambda$ and Eqs. (32) and (33) will degenerate to Eqs. (42) and (43) in Ref. [31], respectively.

3. Numerical examples and discussions

In this section, the propagation behavior of flexural waves in an infinite prestressed smart LR beam will be studied numerically and the attentions will be focused on the tunability of band gaps by adjusting the axial force and AECAs. The parameters of the smart LR beam are taken as follows: $E = 76.92$ GPa, $\rho = 2700$ kgm^{-3}, $H = 0.002$ m, $L = 0.1$ m, $b = 0.1$ m, $m_R = 0.027$ kg, and $k_{ss} = 0.9593 \times 10^5$ Nm^{-1}. To make the problem more clear, we further introduce the relative magnitude of the active stiffness of the piezoelectric spring, $\eta_{as} = k_{as}/k_{ss}$, and the dimensionless axial force $\bar{N} = N/EA$.

To validate the present theoretical derivation and numerical calculation, we here perform a comprehensive comparison. Firstly, the degenerated case where no control actions are applied (i.e., $\bar{N} = 0$ and $\eta_{as} = 0$) is examined. The band structure calculated by Eq. (26) and that extracted from Figure 2a in Ref. [31] are plotted together in Figure 2. It is seen that the present theoretical results agree quite well with the existing ones for the nonprestressed passive beam. On the other hand, the results obtained by TMM and the plane wave expansion method (PWEM) [31] are also shown in Figure 3 for a prestressed passive beam with $\bar{N} = 3.25 \times 10^{-4}$ and $\eta_{as} = 0$. In the calculation by PWEM, we have used 121 plane waves in order to achieve a good convergence of the results. It can be found that the results calculated by the two methods are almost identical, which again validates the TMM .

To clearly show the effect of the applied axial force on the band structure, we combine the curves in Figures 2 and 3 together, and the results are shown in Figure 4. In each case ($\bar{N} = 0$ or $\bar{N} = 3.25 \times 10^{-4}$), there are two band gaps, denoted as g_1 (the lower band gap) and g_2 (the higher band gap), respectively. When the LR beam is stretched by an axial force, the lower edge of g_1 is upraised while the upper edge of g_1 almost keeps unchanged. Consequently, the gap width of g_1 is narrowed. On the other hand, the lower and upper edges of g_2 are both raised up by the tensile force, but the width of g_2 is narrowed. It is worth noting that gap g_2 represents the Bragg gap due to its strong dependance on N, while gap g_1 represents the LR gap since its frequency range is not sensitive to N_1. In fact, the resonance frequency of the resonators in this example is $\omega_R/2\pi = 300$ Hz, which locates within g_1, and the first order Bragg frequency is $\omega_{B1}/2\pi = 484.1$ Hz (for

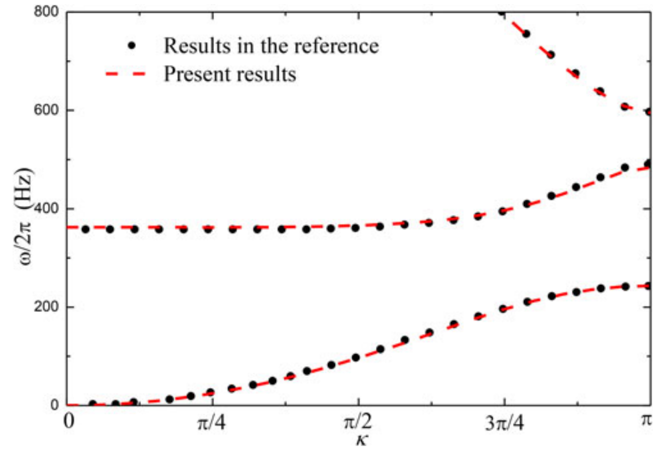

Figure 2. Comparison between the present results and the results in Ref. [31].

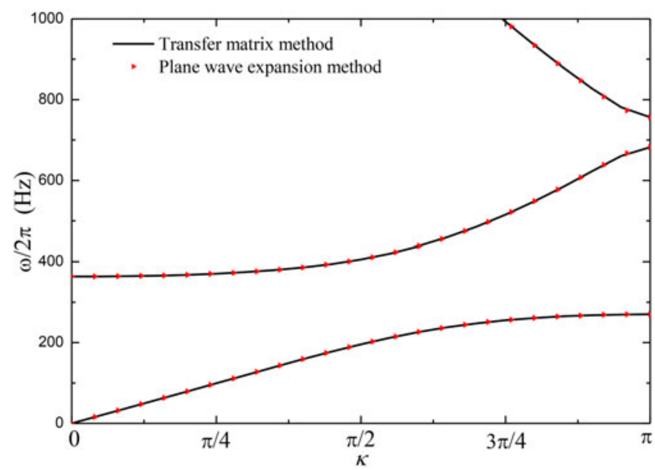

Figure 3. Comparison between the TMM and the PWE method.

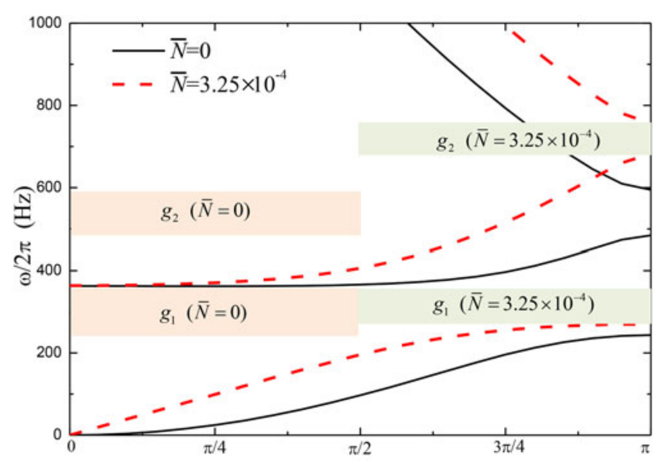

Figure 4. The influence of axial force on the band structure.

$\bar{N} = 0$) or $\omega_{B1}/2\pi = 682.5$ Hz (for $\bar{N} = 3.25 \times 10^{-4}$), which is the lower GEF of g_2 for each case.

Now, let's turn to discuss the influence of AECAs on the band structure. The dispersion curves of the LR beam with and without AECAs are shown in Figure 5, where the axial force is not considered. It can be observed from Figure 5 that: **1)** the Bragg frequency, which is the lower GEF of g_2, is not affected by the AECA; **2)** the two edges of gap g_1 and

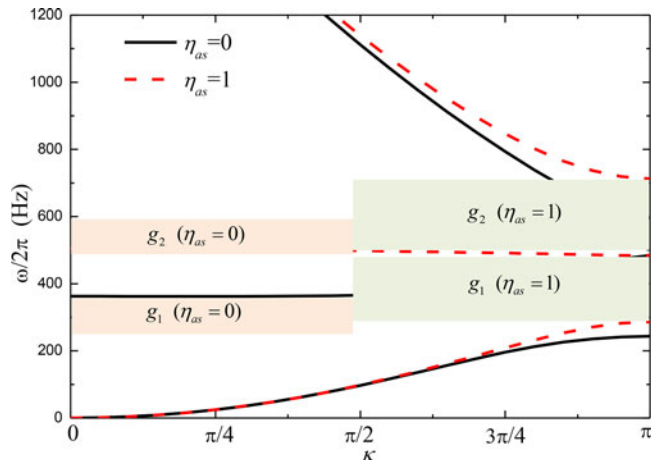

Figure 5. The effect of AECA on the band structure when $\bar{N}=0$.

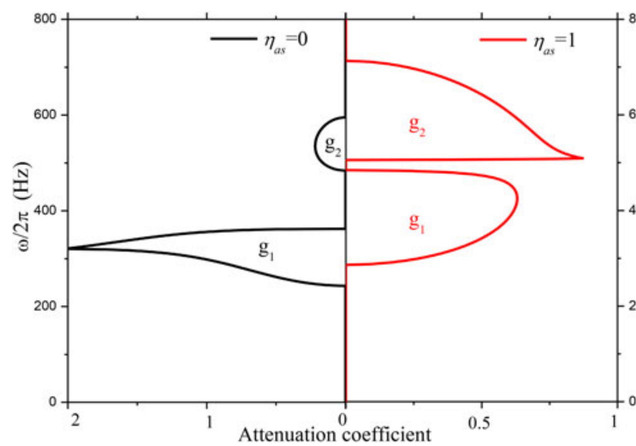

Figure 6. The effect of AECA on the attenuation properties when $\bar{N}=0$. Left panel: $\eta_{as}=0$; right panel: $\eta_{as}=1$.

the higher edge of gap g_2 are all raised up by the AECA; **3)** the gap widths of g_1 and g_2 are broadened, but the width of the pass band between the two band gaps gets narrowed.

To clearly understand the effect of the AECA on the characteristics of the gaps, the attenuation properties as functions of ω, which are calculated from Eq. (28), are plotted in Figure 6, where the left panel represents the case of $\eta_{as}=0$, and the right panel represents the case of $\eta_{as}=1$. Here, the axial force is removed. It should be noted that, for a given angular frequency, Eq. (26) has two solutions of wave number k, i.e. Eq. (28). The wave attenuation coefficient is quantified by the smaller imaginary part of wavenumber, i.e. $\mathrm{Im}(k)$ [31], since it represents the less rapidly decaying wave (the evanescent Bloch wave [34, 35]) that carries energy faster. As expected, the edges of the gaps (corresponding to nonzero attenuation coefficients) shown in Figure 6 agree well with those shown in Figure 5. We observe that for the case of $\eta_{as}=0$, the attenuation properties of the two gaps are quite different from each other. Gap g_1 is characterized by a sharp maximum attenuation, but gap g_2 displays a considerably smooth profile of attenuation over the gap range. This feature confirms that gap g_1 is a LR gap while gap g_2 is a Bragg gap [6, 31], and [34]. However, when $\eta_{as}=1$, the phenomena are quite different. We can see that gap g_1 displays a smooth profile (but not as

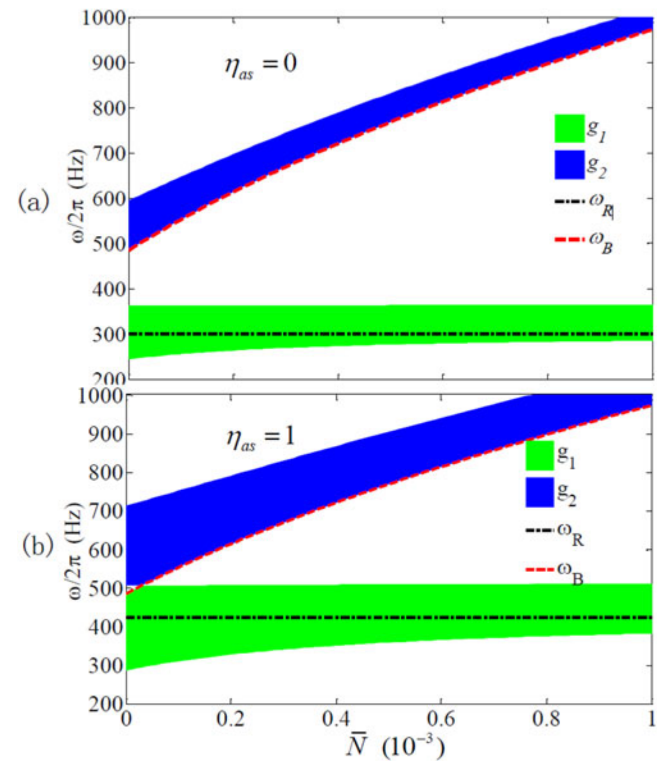

Figure 7. Maps of the two gaps g_1 and g_2 as functions of the axial force. (a): $\eta_{as}=0$; (b): $\eta_{as}=0$.

smooth as that of gap g_2 for $\eta_{as}=0$), while in gap g_2 there exists a sharp maximum attenuation (but not as sharp as that of gap g_1 for $\eta_{as}=0$). Hence, gap g_1 can be regarded as a Bragg-dominant gap and gap g_2 can be considered as a LR-dominant gap. The above results indicate that the natures of the two gaps can be exchanged by applying the AECA.

The foregoing discussions show that both the axial force and the AECA have significant effects on the band structure. For a better knowledge of the dependence of the band gaps on N and η_{as}, we further examine GEFs as functions of these two parameters. With the help of Eqs. (31)–(33), the mappings of band gaps (g_1 and g_2) as functions of the axial force are presented in Figure 7, where Figure 7a and b correspond to $\eta_{as}=0$ and $\eta_{as}=1$, respectively. The red dashed line denotes the first order Bragg frequency ω_{B1} and the black dot-dashed line denotes resonance frequency ω_R. In Figure 7a, i.e. when $\eta_{as}=0$, we observe that ω_R locates in g_1 and the position of g_1 is not sensitive to $\bar{N}$, although its width gets modestly narrowed by the axial force. We also observe that the lower edge of g_2 is determined by the first order Bragg frequency ω_{B1} and its position is significantly increased by $\bar{N}$. Thus we refer to g_1 as the LR gap but regard g_2 as the Bragg gap. In Figure 7b, i.e. when $\eta_{as}=1$, different phenomena can be observed. If the axial force $\bar{N}<\bar{N}^I$, where $\bar{N}^I$ is the critical axial force that makes the pass band between gaps g_1 and g_2 extremely narrow, the upper edge of g_1 is determined by ω_{B1}; but when $\bar{N}>\bar{N}^I$, the lower GEF of gap g_2 is ω_{B1}. Thus we may conclude that when $\bar{N}<\bar{N}^I$ gap g_1 (g_2) is a Bragg (LR) gap, but when $\bar{N}>\bar{N}^I$ the natures of g_1 and g_2 are exchanged. The attenuation properties corresponding to $\bar{N}=0, \eta_{as}=1$ are

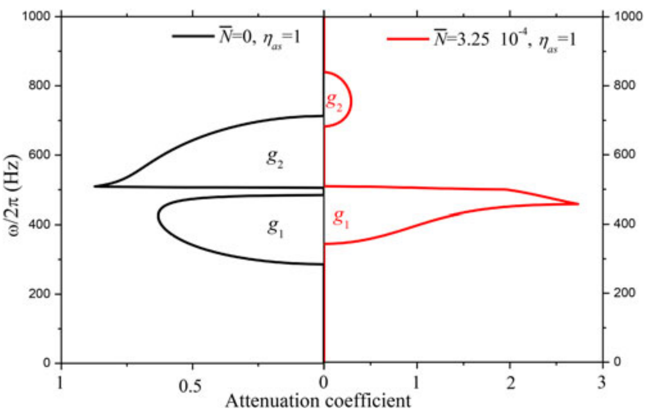

Figure 8. The effect of axial force on the attenuation properties when $\eta_{as} = 1$. Left panel: $\bar{N} = 0$; right panel: $N_1 = 3.25 \times 10^{-4}$.

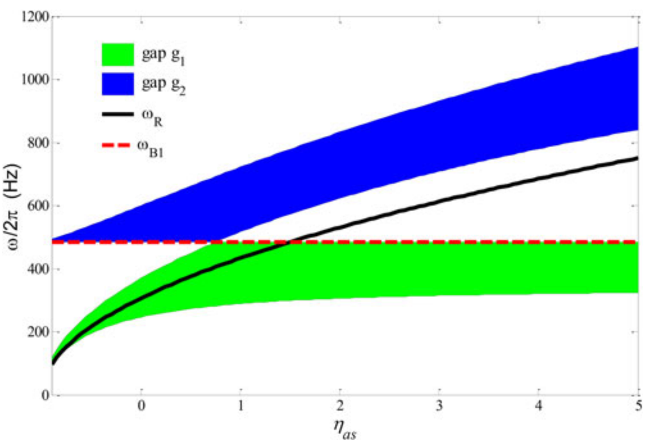

Figure 9. Maps of the two gaps g_1 and g_2 as functions of η_{as} when $\bar{N} = 0$.

presented in the left panel of Figure 8 while those for $\bar{N} = 3.25 \times 10^{-4}, \eta_{as} = 1$ are given in the right panel. It can be observed directly from Figure 8 that the natures of gaps g_1 and g_2 are exchanged by the axial force.

The variations of the band gaps as functions of the ACEA are shown in Figure 9. The green domain denotes gap g_1, the blue domain represents gap g_2, the black dot-dashed line is the resonance frequency of the oscillators, and the red dashed line represents the first order Bragg frequency. We can observe the following phenomena. When $\eta_{as} < \eta_{as}^I$, where η_{as}^I is the critical electrical control parameter making the pass band between the two gaps g_1 and g_2 extremely narrow, the resonance frequency ω_R locates in gap g_1, and the position of g_1 increases with η_{as}. We also observe that the lower GEF of g_2, determined by the first order Bragg frequency ω_{B1}, remains unchanged. Thus when $\eta_{as} < \eta_{as}^I$, gap g_1 can be regarded as the LR gap while gap g_2 can be considered as the Bragg gap. This point has been proved by the left panel of Figure 6. On the other hand, when $\eta_{as} > \eta_{as}^I$, it is observed that the higher GEF of g_1 is ω_{B1} and remains unchanged, while the frequency range of g_2 increases with η_{as}. Therefore we can regard gap g_1 as the Bragg gap and gap g_2 as the LR gap if $\eta_{as} > \eta_{as}^I$. This point has also been proved by the right panel of Figure 6.

Surprisingly, we observe that ω_R will locate in the Bragg gap or even in the pass band. To explain this seemingly strange phenomenon, we take $\eta_{as} = 2$ and $\bar{N} = 0$ as an

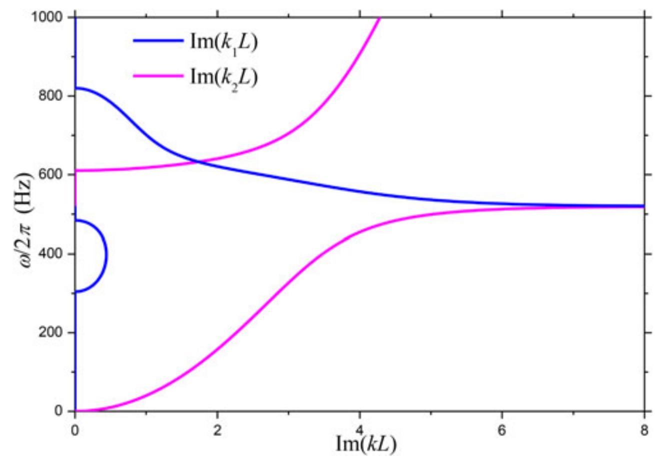

Figure 10. Imaginary parts of the wavenumbers when $\bar{N} = 0$ and $\eta_{as} = 2$.

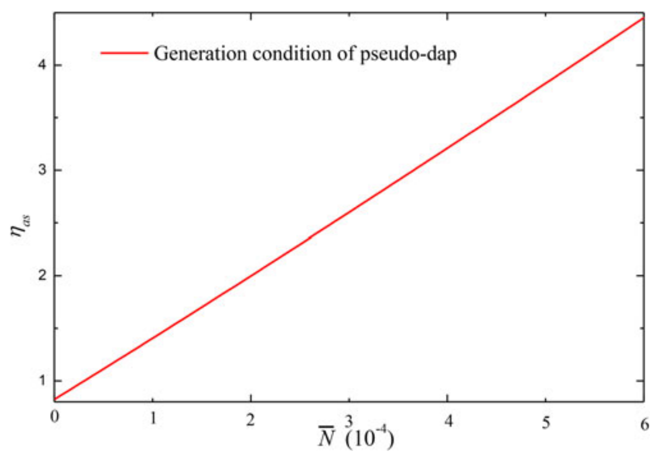

Figure 11. Generation condition of super-wide pseudo-gap.

example and present the imaginary parts of wavenumbers in Figure 10. It is seen that there are two limiting trends: $\lim_{\omega\to\omega_R^+}[\mathrm{Im}(k_1L)] \to 0$ and $\lim_{\omega\to\omega_R^-}[\mathrm{Im}(k_2L)] \to 0$. These two limits lead to $\lim_{\omega\to\omega_R^-}\theta \to 0$ and $\lim_{\omega\to\omega_R^+}\theta \to 0$, where θ denotes the attenuation coefficient. Thus, we can conclude that the resonance frequency and its neighboring frequencies locate in the pass band in this situation.

In Figures 7b and 9, we observe that in some special situations, the pass band between the two gaps g_1 and g_2 will become extremely narrow, and a super-wide pseudo-gap, as a combination of the LR and Bragg gaps, then emerge. This phenomenon is very similar to that reported in Ref. [31]. The generation condition of such pseudo-gap is found to be

$$\eta_{as} = \frac{2EIm_R(\pi^2+\Gamma^2)\pi^2\Gamma^2}{2(\pi^2+\Gamma^2)k_{ss}\rho AL^4 + k_{ss}m_R\pi^2\Gamma L^3\coth(\Gamma/2)} - 1 \quad (34)$$

where

$$\Gamma = \sqrt{\pi^2 + \bar{N}AL^2/I} \quad (35)$$

The relation between η_{as} and $\bar{N}$ is presented in Figure 11. It is shown that the generation condition of such pseudo-gap is presented by an almost linear relation between η_{as} and $\bar{N}$.

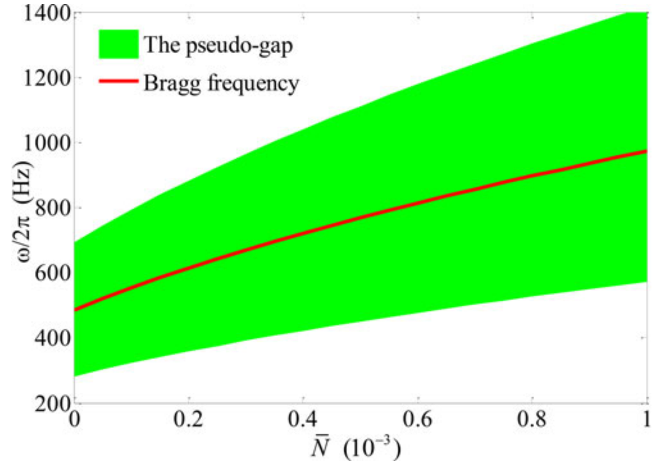

Figure 12. Mapping of the super-wide pseudo-gap as a function of $\bar{N}$.

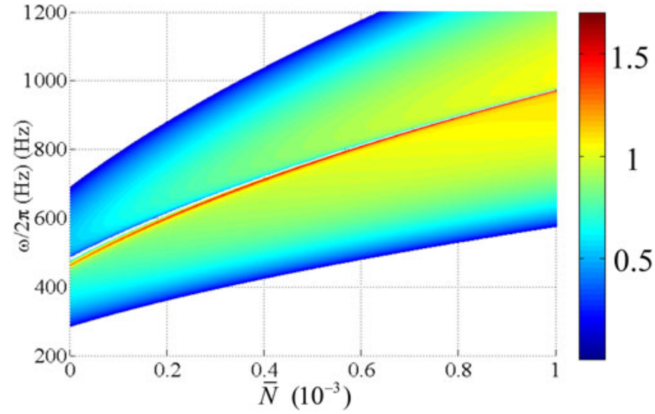

Figure 13. Contours of the attenuation properties of the super-wide pseudo-gap as a function of $\bar{N}$ and frequency.

Figure 12 shows the mapping of the super-wide pseudo-gap as a function of $\bar{N}$. Remind that the active stiffness (η_{as}) should also be controlled simultaneously in a way following the relation (34). Here, the green domain is the pseudo-gap range, the black dot-dashed line denotes resonance frequency ω_R, and the red dashed line represents the first order Bragg frequency ω_{B1}. We observe that both the location and the gap width of the pseudo-gap increase with the axial force $\bar{N}$. The contours of the attenuation properties of such pseudo-gap in the $\bar{N}-\omega$ plane are presented in Figure 13, in which the amplitudes are distinguished by colors. It can be seen that there is an extremely narrow pass band (denoted as white range) locating at almost the center of the pseudo-gap range, and the maximum attenuation coefficient locates below but near this pass band.

As a conclusion, by simultaneously applying the axial force and AECA that meet the condition (34), an actively tunable super-wide pseudo-gap can be achieved.

4. Conclusion

In this paper, we have investigated the tunable band gaps in a prestressed elastic beam with periodically attached piezoelectric spring-mass resonators. The AECA is employed to tune the stiffness of the piezoelectric spring. By using the transfer matrix method, the dispersion relation of the system is obtained in a simple and explicit form, which is a quadric equation of $\cosh(ikL)$. Then two explicit solutions of $k(\omega)$ are solved from the dispersion equation, which can be used to quantify the wave attenuation performance of the band gaps. Furthermore, the GEFs are given explicitly to establish the band gap ranges.

Numerical examples show that the LR gap and Bragg gap coexist in the stretched smart LR beam owing to the coexistence of the LR and structural periodicity. We also find that, by changing the axial force and/or the AECA, the width and location of both the LR gap and Bragg gap can be tuned actively. Furthermore, the natures of the two neighboring band gaps may be exchanged. In particular, a super-wide pseudo-gap formed by a combination of the LR gap and Bragg gap will emerge if the axial force and the ACEA are applied appropriately. Inside the pseudo-gap, there is an extremely narrow pass band. The generation condition of such pseudo-gap is further obtained, which explicitly relates the AECA to the axial force. Then by tuning the axial force and the AECA simultaneously, the broad pseudo-gap can be actively controlled provided that the derived condition is met. The present study can help us understand the behavior of the actively tunable LR beam, and promise many potential applications in the fields including vibration isolators, frequency filters, and new smart transducers. In addition, the super-narrow pass band located in a wide pseudo-gap may provide a new method to design actively tunable selectors of pure frequency.

Disclosure statement

No potential conflict of interest was reported by the authors.

Funding

The work was supported by the National Natural Science Foundation of China (Nos. 11532001, 11621062 and 11402310). Partial support from the Fundamental Research Funds for the Central Universities (No. 2016XZZX001-05) is also acknowledged.

References

[1] M. S. Kushwaha, P. Halevi, L. Dobrzynski, and B. Djafari-Rouhani, “Acoustic band structure of periodic elastic composites,” Phys. Rev. Lett., vol. 71, no. 13, pp. 2022–2025, 1993.
[2] M. M. Sigalas and E. N. Economou, “Elastic and acoustic wave band structure,” J. Sound Vibration, vol. 158, no. 2, pp. 377–382, 1992.
[3] H. Zhao, Y. Liu, D. Yu, G. Wang, J. Wen, and X. Wen, “Absorptive properties of three-dimensional phononic crystal,” J. Sound Vibration, vol. 303, no. 1–2, pp. 185–194, 2007.
[4] J. S. Jensen, “Phononic band gaps and vibrations in one-and two-dimensional mass–spring structures,” J. Sound Vibration, vol. 266, no. 5, pp. 1053–1078, 2003.
[5] Z. Q. Zhan and P. J. Wei, “Band gaps of three-dimensional phononic crystal with anisotropic spheres,” Mech. Adv. Mater. Struct., vol. 21, no. 4, pp. 245–254, 2014.

[6] Z. Liu *et al.*, “Locally resonant sonic materials,” Science, vol. 289, no. 5485, pp. 1734–1736, 2000.

[7] H. Zhang, Y. Xiao, J. Wen, D. Yu, and X. Wen, “Flexural wave band gaps in metamaterial beams with membrane-type resonators: theory and experiment,” J. Phys. D: Appl. Phys., vol. 48, no. 43, pp. pp. 435305, 2015.

[8] J. Li, and C. T. Chan, “Double-negative acoustic metamaterial,” Phys Rev E Stat Nonlinear Soft Matter Phys., vol. 70, no. 5 Pt 2, pp. 055602, 2004.

[9] J. Z. Sun and P. J. Wei, P J. “Band gaps of 2D phononic crystal with imperfect interface,” Mech. Adv. Mater. Struct., vol. 21, no. 2, pp. 107–116, 2014.

[10] Z. Liu, C. T. Chan, and P. Sheng, “Analytic model of phononic crystals with local resonances,” Phys. Rev. B, vol. 71, no. 1, pp. 014103, 2005.

[11] S. Zhang, L. Yin, and N. Fang, “Focusing ultrasound with an acoustic metamaterial network,” Phys. Rev. Lett., vol. 102, no. 19, pp. 194301, 2009.

[12] Z. Yang, J. Mei, M. Yang, N. H. Chan, and P. Sheng, “Membrane-type acoustic metamaterial with negative dynamic mass,” Phys. Rev. Lett., vol. 101, no. 20, pp. 204301, 2008.

[13] G. Wang, X. Wen, J. Wen, L. Shao, and Y. Liu, “Two-dimensional locally resonant phononic crystals with binary structures,” Phys. Rev. Lett, vol. 93, no. 15, pp. 154302, 2004.

[14] N. Fang *et al.*, “Ultrasonic metamaterials with negative modulus,” Nat. Mater., vol. 5, no. 6, pp. 452–456, 2006.

[15] S. H. Lee, C. M. Park, Y. M. Seo, Z. G. Wang, and C. K. Kim, “Acoustic metamaterial with negative modulus,” J. Phys. Condens. Matter., vol. 21, no. 17, pp. 175704, 2009.

[16] H. H. Huang, C. T. Sun, and G. L. Huang, “On the negative effective mass density in acoustic metamaterials,” Int. J. Eng. Sci., vol. 47, no. 4, pp. 610–617, 2009.

[17] K. Bertoldi, and M. C. Boyce, “Wave propagation and instabilities in monolithic and periodically structured elastomeric materials undergoing large deformations,” Phys. Rev. B, vol. 78, pp. 184107, 2008.

[18] Y. Huang, X. D. Shen, C. L. Zhang, and W. Q. Chen, “Mechanically tunable band gaps in laminated composites with finite deformation,” Phys. Lett. A, vol. 378, no. 30–31, pp. 2285–2289, 2014.

[19] E. G. Barnwell, W. J. Parnell, and I. D. Abrahams, “Antiplane elastic wave propagation in pre- eriodic structures; tuning, band gap switching and invariance,” Wave Motion, vol. 63, pp. 98–110, 2016.

[20] P. Galich and S. Rudykh, “Manipulating pressure and shear elastic waves in dielectric elastomers via external electric stimuli,” Int. J. Solids Struct., vol. 91, pp. 18–25, 2016.

[21] M. Gei, S. Roccabianca, and M. Bacca, “Controlling bandgap in electroactive polymer-based structures,” Mechatronics, IEEE/ASME Trans. Mech., vol. 16, no. 1, pp. 102–107, 2011.

[22] R. Getz, D. M. Kochmann, and G. Shmuel, “Voltage-controlled complete stopbands in two-dimensional soft dielectrics,” Int. J. Solids Struct., vol. 113–114, pp. 24–36, 2017.

[23] M. Destrade, and R. W. Ogden, “On magneto-acoustic waves in finitely deformed elastic solids,” Math. Mech. Solids, vol. 16, no. 6, pp. 594–604, 2011.

[24] M. Gei, A. B. Movchan, and D. Bigoni, “Band-gap shift and defect-induced annihilation in prestressed elastic structures,” J. Appl. Phys., vol. 105, no. 6, pp. 063507, 2009.

[25] P. L. Galich, N. X. Fang, M. C. Boyce, and S. Rudykh, “Elastic wave propagation in finitely deformed layered materials,” J. Mech. Phys. Solids, vol. 98, pp. 390–410, 2017.

[26] K. Bertoldi, M. C. Boyce, S. Deschanel, S. M. Prange, and T. Mullin, “Mechanics of deformation-triggered pattern transformations and superelastic behavior in periodic elastomeric structures,” J. Mech. Phys. Solids, vol. 56, no. 8, pp. 2642–2668, 2008.

[27] V. Slesarenko and S. Rudykh, “Harnessing viscoelasticity and instabilities for tuning wavy patterns in soft layered composites,” Soft Matter, vol. 12, no. 16, pp. 3677–3682, 2016.

[28] S. Rudykh and M. C. Boyce, “Transforming wave propagation in layered media via instability-induced interfacial wrinkling,” Phys. Rev. Lett., vol. 112, no. 3, pp. 034301, 2014.

[29] S. Babaee, N. Viard, P. Wang, N. X. Fang, and K. Bertoldi, “Harnessing deformation to switch on and off the propagation of sound,” Adv. Mater. Weinheim, vol. 28, no. 8, pp. 1631–1635, 2016.

[30] A. Baz, “Active control of periodic structures,” J. Vibration Acoust., vol. 123, no. 4, pp. 472–479, 2001.

[31] Y. Xiao, J. Wen, and X. Wen, “Flexural wave band gaps in locally resonant thin plates with periodically attached spring-mass resonators,” J. Phys. D Appl. Phys., vol. 45, no. 19, pp. 195401, 2012.

[32] Y. Xiao, B. R. Mace, J. Wen, and X. Wen, “Formation and coupling of band gaps in a locally resonant elastic system comprising a string with attached resonators,” Phys. Lett. A, vol. 375, no. 12, pp. 1485–1491, 2011.

[33] C. Kittel, Introduction to Solid State Physics. New York: Wiley, 1986.

[34] D. J. Mead, “Wave propagation and natural modes in periodic systems: I. Mono-coupled systems,” J. Sound Vibration, vol. 40, no. 1, pp. 1–18, 1975.

[35] V. Romero-Garcia, J. V. Sanchez-Perez, S. Castineira-Ibanez, and L. M. Garcia-Raffi, “Evidences of evanescent Bloch waves in phononic crystals,” Appl. Phys. Lett., vol. 96, no. 12, pp. 124102, 2010.